THE JOURNAL OF PHYSICAL CHEMISTRY A
A JOURNAL OF THE AMERICAN CHEMICAL SOCIETY

pubs.acs.org/JPCA

Article

Energy Transfer Mechanism and Quantitative Modeling of Rate from an Antenna to a Lanthanide Ion

Peter A. Tanner,* Waygen Thor, Yonghong Zhang, and Ka-Leung Wong*

Cite This: *J. Phys. Chem. A* 2022, 126, 7418−7431

Read Online

ACCESS | Metrics & More | Article Recommendations | Supporting Information

ABSTRACT: The excitation energy transfer (ET) pathway and mechanism from an organic antenna to a lanthanide ion has been the subject of discussion for many decades. In the case of europium (Eu^{3+}), it has been suggested that the transfer originates from the ligand singlet state or a triplet state. Taking the lanthanide complex $\mathbf{Eu(TTA)_3(H_2O)_2}$ as an example, we have investigated the spectra and luminescence kinetics, mainly at room temperature and 77 K, to acquire the necessary experimental data. We put forward an experimental and theoretical approach to measure the energy transfer rates from the antenna to different Eu^{3+} levels using the Dexter formulation. We find that transfer from the ligand singlet state to Eu^{3+} may account for the ET pathway, by combined electric dipole−electric dipole (ED−ED) and ED-electric quadrupole (EQ) mechanisms. The contributions from the triplet state by these mechanisms are very small. An independent systems rate equation approach can effectively model the experimental kinetics results. The model utilizes the cooperative processes that take place on the metal ion and ligand and considers S_0, S_1, and T_1 ligand states in addition to $^7F_{0,1}$, $^5D_0$, $^5D_1$, and ^5DJ (=$^5L_6$, $^5D_3$, $^5D_2$ combined) Eu^{3+} states. The triplet exchange ET rate is estimated to be of the order 10^7 s^{-1}. The observation of a nanosecond risetime for the Eu^{3+} $^5D_1$ level does not enable the assignment of the ET route or the mechanism. Furthermore, the $^5D_1$ risetime may be contributed by several processes. Observation of its temperature dependence and also that of the ground-state population can supply useful information concerning the mechanism because the change in metal-ion internal conversion rate has a greater effect than changes in singlet or triplet nonradiative rates. A critical comparison is included for the model of Malta employed in the online software LUMPAC and JOYSpectra. The theoretical treatment of the exchange mechanism and its contribution are now being considered.

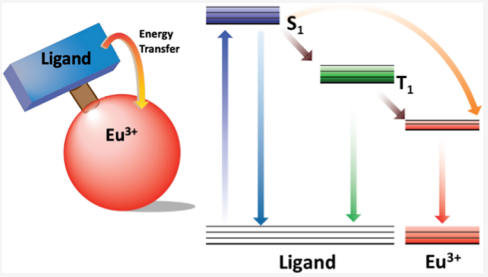

INTRODUCTION

Lanthanide ions are versatile lighting and display elements, but their performance relies upon an efficient antenna because their absorption is very weak. Hence, there have been many thousands of papers describing the quantum efficiency and brightness of their complexes with organic ligands, particularly for europium, Eu^{3+}. From experiment, some studies have proposed that the singlet state S_1 (or a charge transfer (CT) state) is responsible for the transfer of energy from the coordinated ligand to the Eu^{3+} energy levels,[1−5] whereas the majority of reports consider that energy transfer (ET) occurs from the ligand triplet state, T_1[6−8] (Figure 1a). The understanding of the major ET pathway and mechanism is particularly important for the development and optimization of photovoltaic and optoelectronic devices, such as in lighting and displays, light-emitting diodes (LEDs), biomarkers, sensors, fluoroimmunoassays, and noncontact thermometers.[9−13]

Naturally, the Eu^{3+} population mechanism can depend upon many factors including the type of ligand system. However, confirmatory evidence from experiment should show that the Eu^{3+} acceptor luminescence risetime is equal to the *donor* decay time. Moreover, even the confirmation of the energy transfer route may not be sufficient to elucidate the relevant mechanism.[6]

Hence, attempts to unravel the population channel and its mechanism have turned to theory. However, to date, there has only been a comprehensive quantitative description given by Malta and co-workers[12,16−18] for the transfer of energy from the antenna to the Eu^{3+} metal ion. The model of Malta, using the tensor operator techniques of Kushida,[19] has been employed in many publications and has sometimes concluded that singlet ET occurs to Eu^{3+}, and in other cases, triplet ET occurs. The earlier publications evidently overestimated the contributions from exchange ET. The model is available for use in free and widely used computation software programs called LUMPAC[20] and JOYSpectra.[21]

The key question which has been targeted in many publications is: does the antenna ET originate from a singlet or a triplet channel? Naturally, both can contribute to varying extents. We present an alternative strategy for attacking this

Received: June 8, 2022
Revised: September 12, 2022
Published: October 6, 2022

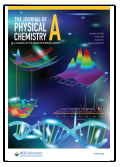

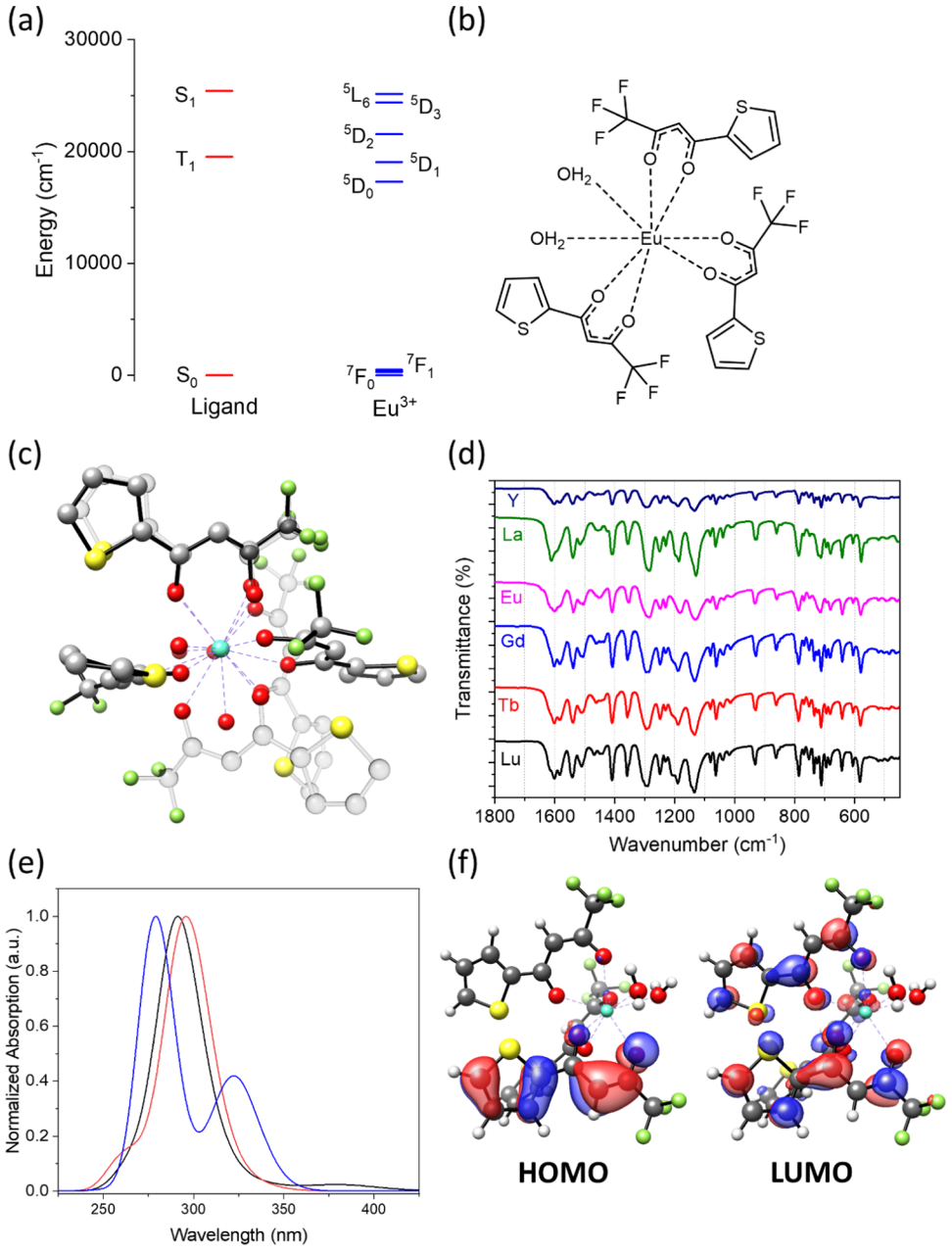

Figure 1. (a) Selected energy levels of the ligand-Eu^{3+} system. (b) Schematic structure of the complex. (c) X-ray structure of triclinic Isomer I of $\mathbf{Eu(TTA)_3(OH_2)_2}$ showing the disorder of the thienyl group in one of the coordinated TTA ligands[14] (black bonds) superimposed upon Isomer II, the monoclinic structure[15] (gray bonds). (d) Infrared spectra of $\mathbf{Ln(TTA)_3(OH_2)_2}$ complexes. (e) Calculated ultraviolet absorption spectra using time-dependent density functional theory (TD-DFT) for $\mathbf{Eu(TTA)_3(OH_2)_2}$ in the gas phase (black) and in toluene solution (red). The MWB52-PBE0/D3BJ/def2-TZVP level of theory was employed, and the CPCM model was employed for the solution spectrum. The CASSCF-NEVPT2 calculated spectrum using a (6,6) active space is shown in blue. (f) DFT frontier orbitals of $\mathbf{Eu(TTA)_3(OH_2)_2}$ in toluene solution.

question which utilizes experimental data in conjunction with theory. The compound $\mathbf{Eu(TTA)_3(H_2O)_2}$ (TTA = thenoyltrifluoroacetonate) (Figure 1b) has been chosen for the demonstration of the results because it has been widely studied and applied,[8,22−28] and it has been used for illustration in the software JOYSpectra.[21] The temporal variation of the populations of ligand and metal states has been reproduced by a new rate equation model.

METHODS

Materials. $\mathbf{EuCl_3{\cdot}6H_2O}$ and $\mathbf{LaCl_3{\cdot}7H_2O}$ were purchased from Sigma-Aldrich (≥99.99% trace-metal basis) and used without further purification. All organic chemicals were purchased from TCI or Energy Chemical with 98% purity and used without further purification.

Synthesis. $\mathbf{Ln(TTA)_3(H_2O)_2}$ were obtained according to a procedure following the literature method.[24] Briefly, for Ln = Eu, **HTTA** (0.67 g, 3 mmol) was dissolved in 15 mL of ethanol in a 150 mL flask, with stirring at room temperature. Then, the pH of the solution was adjusted to 6−7 by the addition of **NaOH** solution (1.0 M). After that, 1 mmol of $\mathbf{EuCl_3{\cdot}6H_2O}$ (0.37 g, 1 mmol) solution in 5.0 mL of deionized water was added to the above mixture at 60 °C. Then, deionized water (100 mL) was added to the above mixture with vigorous stirring for 2 h at 60 °C

https://doi.org/10.1021/acs.jpca.2c03965
J. Phys. Chem. A 2022, 126, 7418−7431

to ensure complete precipitation. After cooling to room temperature, the precipitate was filtered, washed repeatedly with water, and dried overnight under vacuum at room temperature to afford $\mathbf{Eu(TTA)_3(H_2O)_2}$ as a light yellow solid (0.68 g, 80%). $\mathbf{Ln(TTA)_3(H_2O)_2}$ (Ln = Gd, La) were prepared analogously. The compound easily decomposes in a moist atmosphere. The results of thermogravimetric analysis are shown in Figure S1.

Instruments. Excitation and emission spectra and luminescence decay curves were obtained by a Fluorolog-3 spectrometer from Horiba with a 450 W Xenon lamp, Horiba Nano, and Spectra LEDs as excitation sources. Spectra were recorded at 77 K with the samples in NMR tubes in a home-built liquid nitrogen setup made of glass. Experiments at the sensor reading of 10 K (i.e., the nominal 10 K temperature) were performed using an Optical Cryostat-CS202I-DMX-1SS from Advanced Research Systems Instruments, Inc. Emission spectra with higher resolution were also measured using an iHR 550 spectrometer with a system consisting of a Nd:YAG pump laser, a third-order harmonic generator (THG at 355 nm, 120 mJ), and an optical parameter oscillator (OPO, Spectra-Physics VersaScan, and UVScan) with a pulse duration of 8 ns and repetition frequency of 10 Hz. Absorption spectra were recorded at room temperature for solutions in quartz cuvettes using a PerkinElmer LAMBDA 1050+ UV/VIS/NIR double-beam spectrophotometer. A qX3/Horiba4 variable-temperature cell was employed to investigate the temperature dependence of emission between 280 and 323 K. A 10 mm pathlength cuvette was used for all room-temperature measurements. Fourier transform infrared (FT-IR) spectra were recorded using a PerkinElmer FT-IR Spectrum Two equipped with $LiTaO_3$ detector.

Computation of Molecular Structure and State Energies. Rate Equations. Calculations were performed using Orca version 4.2.1[29,30] and accessories, together with the use of Avogadro[31,32] and Gabedit.[33] In these density functional theory (DFT) calculations, the PBE0[34,35] functional was employed with the def2-TZVP basis set,[36] with the Stuttgart in-core effective core potential and basis set for Eu^{3+}.[37,38] In all optimizations, the Grimme dispersion correction D3BJ was used.[39,40] The calculation for $\mathbf{Eu(TTA)_3(H_2O)_2}$ in toluene solvent used the Conductor-like Polarizable Continuum Model (CPCM).[41] The optimized structures were checked to represent true minima by calculation confirming the absence of imaginary frequencies. The simulated absorption spectra employed a bandwidth of 2000 cm^{-1}. The time-dependent DFT calculation employed 30 roots. Molecular orbital figures used the isosurface values of 0.05 e/a_0^3 in all cases.

CASSCF-NEVPT2 calculations[42−44] were also performed using ORCA 4.2.1. for 10 roots, following a second-order Møller−Plesset theory calculation with the optimized structure from the above DFT. The basis set 6-31+G(d)[45] was used for all atoms except Eu, with the auxiliary basis: def2-TZVP/C.[46]

Multiwfn v3.7.[47] was used to determine the molecular orbital coefficients at atomic positions. Distances from Eu to the relevant atoms were measured in Diamond[48] and Avogadro.[31,32]

The wavefunction for $^7F_0$ (or $^5D_0$, for example) comprises several other SLJ multiplets in the intermediate coupling scheme. For example, for Eu^{3+} in $\mathbf{Lu_2O_3}$, the wavefunction of $^7F_0$ due to J-mixing is[49]

$$85.5\%|^7F\ 0\ 0\rangle + 3.0\%|^5D(1)0\ 0\rangle + 2.7\%|^7F\ 2\ 2\rangle + 2.7\%|^7F\ 2{-}2\rangle + 2.6\%|^5D(3)0\ 0\rangle + \ldots$$

where the two numbers after the term represent J and M_J values. Hence, there is about a 5% contribution to the $^7F_0$ wavefunction from $^7F_2$ and this has been recognized in the reduced matrix elements given by Kasprzycka et al.[50] Ideally, this contribution should be included in calculations, but for simplicity, we restrict our calculations to mainly order-of-magnitude results.

Maple 2021[51] was employed for computations involving the rate equation model.

THEORETICAL BACKGROUND

The oscillator strength P_{if} of a transition between initial (i) and final (f) states of a system is measured experimentally from an emission spectrum if the low-temperature lifetime τ is approximated as the radiative lifetime τ_R, as[52,53]

$$P_{if} = \frac{4\pi\varepsilon_0}{\tau_R}\frac{mc^3}{8e^2\pi^2\nu^2}\left\{\frac{\varepsilon_{macr}}{\varepsilon_{loc}}\right\}^2\frac{1}{n} \tag{1a}$$

or

$$P_{if} = 1.4992 \times 10^{-14}\frac{\lambda^2}{\tau_R} \times \chi \tag{1b}$$

where the virtual cavity model correction for the macroscopic and local electric field has been inserted in (eq 1b) for an electric dipole (ED)-allowed transition $\chi_{ED} = \frac{9}{n(n^2+2)^2}$ or $\chi_{MD} = n^3$ for a magnetic dipole (MD)-allowed transition; ε_0 (F m^{-1}) is the vacuum permittivity, ν (s^{-1}) is the transition frequency, c is the speed of light (m s^{-1}), m is the electron mass (kg), λ is the emission wavelength (in nm), n is the refractive index, and τ_R (s) = $1/A$ is the radiative lifetime (A is the Einstein coefficient of spontaneous emission, s^{-1}).

Alternatively, the oscillator strength can be approximately measured from the absorption spectrum: from the linear absorption coefficient α (m^{-1}) or the absorption cross section σ (m^2), where N (m^{-3}) is the number of absorbing centers per unit volume, and i and f are the initial and final levels in the transition

$$Q_{if} = \frac{\int\alpha(E)\mathrm{d}E}{N} = \int\sigma(E)\mathrm{d}E \tag{2}$$

$$P_{if} = 4\pi\varepsilon_0 Q_{if}\frac{mcn}{h\pi e^2}\left\{\frac{\varepsilon_{macr}}{\varepsilon_{loc}}\right\}^2 \tag{3}$$

Here, h is Planck's constant (J s) and $E = h\nu$. Hence, in terms of $\overline{\nu}$ (cm^{-1})

$$P_{if} = 1.017 \times 10^{15}\frac{n}{N(n^2+2)^2}\int\alpha(\overline{\nu})\mathrm{d}\overline{\nu} \tag{4}$$

or in terms of molar absorption coefficient, ε (mol^{-1} cm^{-1} dm^3)

$$P_{if} = 4.319 \times 10^{-9}\int\varepsilon(\overline{\nu})\mathrm{d}\overline{\nu} \tag{5}$$

where

$$\varepsilon = \frac{1}{lc}\log\frac{P_0}{P} \tag{6}$$

https://doi.org/10.1021/acs.jpca.2c03965
J. Phys. Chem. A 2022, 126, 7418−7431

with l being the pathlength (cm), c the concentration (mol dm^{-3}), and P_0 and P the incident and transmitted power through the sample, respectively. The use of eq 5 pertains to the population of the initial state, which for $^7F_0$ is rather less than 1.

The oscillator strength for an ED-allowed transition can be calculated from the line strength (in C^2 m^2), S_{if} (ED) = $\sum_{i,f}|\langle\varphi_f|\mu_e|\varphi_i\rangle|^2$ of the transition, where μ_e is the ED moment operator

$$P_{if} = \frac{8\pi^2 m\nu}{3he^2}\frac{1}{g_i}S_{if}(\mathrm{ED}) = 4.2257 \times 10^{52}\frac{\overline{\nu}}{g_i}S_{if}(\mathrm{ED}) \tag{7}$$

and g_i is the degeneracy of the initial state (which is usually omitted or often placed in the numerator). Since our cases correspond to nondegenerate ($^7F_0$ and S_1) initial states, we do not go into detail here. In eq 7, $\overline{\nu}$ is the peak maximum in cm^{-1}. For example, from eq 7, if P_{if} (singlet) = 0.5 at 25 000 cm^{-1}, then S_{if} equals 4.7329×10^{-58} C^2 m^2 or 4.2537×10^{-35} esu^2 cm^2. The inclusion of local field effects changes the answer in eq 7 by a factor of ∼3.

The oscillator strengths for the analogous transitions in absorption and emission are related by the state degeneracies

$$P_{if} = \frac{g_f}{g_i}P_{fi} \tag{8}$$

The energy transfer rate by the ED−ED mechanism between the donor (D) and acceptor (A) separated by distance R (see later) can be written

$$W_{\mathrm{ET}}(\mathrm{ED}-\mathrm{ED}) = \left\{\frac{1}{4\pi\varepsilon_0}\right\}^2\frac{3he^4}{8n^4m^2\pi^2\nu^2}\frac{1}{R^6}P_{\mathrm{D}}(\mathrm{ED})P_{\mathrm{A}}(\mathrm{ED}) \times \int f_{\mathrm{D}}(E)f_{\mathrm{A}}(E)\mathrm{d}E \tag{9a}$$

Hence $W_{\mathrm{ET}}(\mathrm{ED}-\mathrm{ED})$

$$= \frac{1.614856 \times 10^{-30}}{n^4\nu^2R^6}P_{\mathrm{D}}(\mathrm{ED})P_{\mathrm{A}}(\mathrm{ED})\int f_{\mathrm{D}}(E)f_{\mathrm{A}}(E)\mathrm{d}E \tag{9b}$$

where the units are ν (s^{-1}) (the average frequency of the transitions involved), R (m), and the overlap integral between the normalized emission and absorption spectra is in J^{-1}.

Now we consider interaction comprising an ED transition of the antenna and an electric quadrupole (EQ) transition of the lanthanide ion. The equation given by Dexter for this interaction, neglecting local field effects, is[54]

$$W_{\mathrm{ET}}(\mathrm{ED}-\mathrm{EQ}) = \frac{3.802 \times 10^{29}}{\nu^8n^6R^8\tau_{\mathrm{D}}\tau_{\mathrm{A}}}\frac{2J'+1}{2J''+1} \times \int f_{\mathrm{D}}(E)f_{\mathrm{A}}(E)\mathrm{d}E \tag{10}$$

which shows an R^{-8} dependence. In terms of line strengths, this can be written as[52]

$$W_{\mathrm{ET}}(\mathrm{ED}-\mathrm{EQ}) = \frac{2\pi}{\hbar}\left\{\frac{1}{4\pi\varepsilon_0n^2}\right\}^2\frac{1}{R^8}S_{\mathrm{ED}}(S_1\rightarrow S_0) \times S_{\mathrm{EQ}}(J''\rightarrow J')\int f_{\mathrm{D}}(E)f_{\mathrm{A}}(E)\mathrm{d}E \tag{11a}$$

$$W_{\mathrm{ET}}(\mathrm{ED}-\mathrm{EQ}) = 4.8127 \times 10^{54}\frac{1}{R^8}S_{\mathrm{ED}}(S_1\rightarrow S_0) \times S_{\mathrm{EQ}}(J''\rightarrow J')\int f_{\mathrm{D}}(E)f_{\mathrm{A}}(E)\mathrm{d}E \tag{11b}$$

where the dipole line strength refers to the ligand and the quadrupole line strength to europium, respectively.

The line strength of an EQ transition (in C^2 m^4) from lower level i to upper level f is given by[55]

$$S_{\mathrm{EQ}}(i\rightarrow f) = \frac{A_{\mathrm{EQ}}(2J_i+1)5h\varepsilon_0}{8\pi^5}\left[\frac{\lambda}{n}\right]^5 = 1.198217 \times 10^{-92}A_{\mathrm{EQ}}(2J_i+1)\left[\frac{\lambda}{n}\right]^5 \tag{12a}$$

where λ is in nm; or in terms of oscillator strength

$$S_{\mathrm{EQ}}(i\rightarrow f) = \frac{225\alpha(2J_i+1)P(i\rightarrow f)_{\mathrm{EQ}}}{112\pi^3a_0^3r^2}\left[\frac{\lambda}{n}\right]^3 = 7.992376 \times 10^{-79}(2J_i+1)P(i\rightarrow f)_{\mathrm{EQ}}\left[\frac{\lambda^3}{n^4}\right] \tag{12b}$$

where α is the fine structure constant, a_0 is the Bohr radius, $\langle r^2\rangle$ is the expectation value of the radial wavefunction for Eu^{3+}, and λ is in nm.

The line strength of a ligand ED transition (in C^2 m^2) from an upper level S_1 to a lower level S_0 (both with spin $S = 0$) is given by[56,57]

$$S_{\mathrm{ED}}(S_1\rightarrow S_0) = \frac{3\varepsilon_0h\lambda^3}{16\pi^3}n\chi A_{\mathrm{ED}}(S_1\rightarrow S_0) = 3.547778 \times 10^{-74}\lambda^3n\chi A_{\mathrm{ED}}(S_1\rightarrow S_0) \tag{13}$$

with λ in nm. For a given transition, the ratio[52,54]

$$\frac{W_{\mathrm{ET}}(\mathrm{ED}-\mathrm{EQ})}{W_{\mathrm{ET}}(\mathrm{ED}-\mathrm{ED})} \sim 1.443\left(\frac{n\lambda}{R}\right)^2\frac{\tau_{\mathrm{A}}(\mathrm{ED})}{\tau_{\mathrm{A}}(\mathrm{EQ})} \tag{14}$$

Values of $A'_{\mathrm{EQ}} = 1/(n^5 \times \tau_{\mathrm{A}}(\mathrm{EQ}))$ for the Eu^{3+} free ion have been tabulated by Dodson and Zia.[55] Values of A'_{EQ} for the transitions $^5D_2 \rightarrow {}^7F_0$ at 21 752 cm^{-1} (460 nm) and $^5G_2 \rightarrow {}^7F_0$ at 26 423 cm^{-1} (378 nm) are largest for those under consideration herein, with magnitudes of 3.14×10^{-3} and 4.92×10^{-3} s^{-1}, respectively.

The distance R in eqs 9a−11b does not represent the average donor ligand (O)-Eu acceptor distance, but rather it is the electronic barycenter of the donor state, and the coefficients (c_i) of the donor singlet or triplet molecular orbital at each atom i can be calculated by the Hirshfeld method using Multiwfn 3.7.[47] The value of R is then

$$R = \frac{\sum_i c_i^2R_i}{\sum_i c_i^2} \tag{15}$$

where R_i is the distance from atom i to Eu. We employed the results from our TD-DFT calculation, in addition to a second-order Møller−Plesset (MP2) perturbation calculation, of the orbital compositions of the ligand singlet and triplet states. The calculated values of R, in Å, for the singlet state are TD-DFT 3.79, MP2 4.56; and for the triplet state are TD-DFT 3.96, MP2 4.45. The value given in most publications[12] is 4.5, and we prefer to use this value for reference since it basically agrees with our MP2 calculation results.

https://doi.org/10.1021/acs.jpca.2c03965
J. Phys. Chem. A 2022, 126, 7418−7431

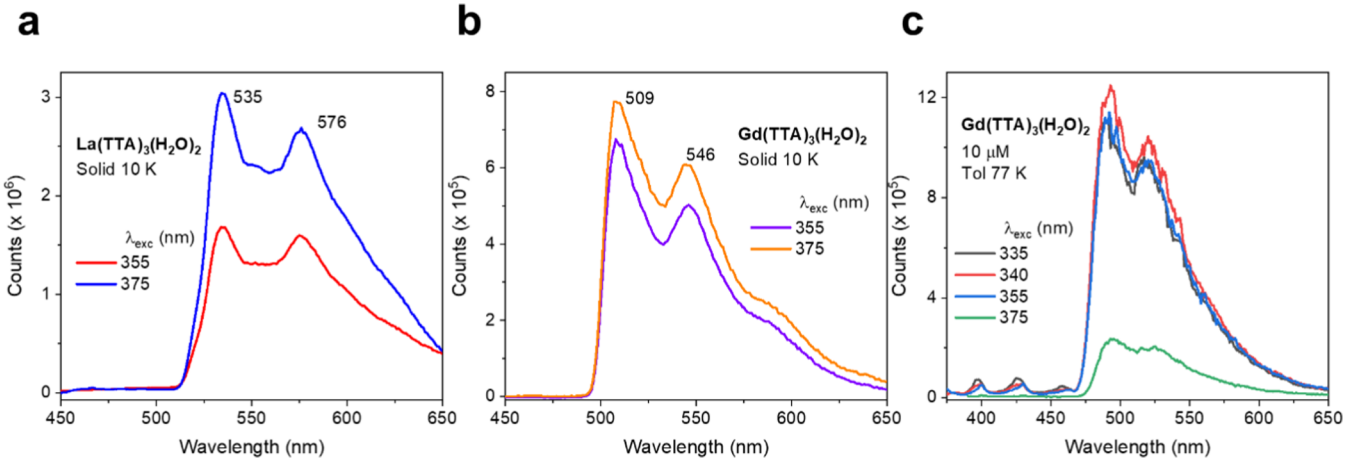

Figure 2. Phosphorescence spectra of solid (a) $\mathbf{La(TTA)_3(H_2O)_2}$ and (b) $\mathbf{Gd(TTA)_3(H_2O)_2}$ at the nominal temperature of 10 K. (c) Fluorescence and phosphorescence spectrum of $\mathbf{Gd(TTA)_3(H_2O)_2}$ in toluene at 10 μM concentration at 77 K. Excitation wavelengths (in nm) were used as indicated. The phosphorescence spectra do not exhibit change in wavelength when the excitation wavelength is altered.

Although the free ion selection rules forbid the ED mechanism for the transition (and others) $^5D_0 \rightarrow {}^7F_0$, the transition is usually observed by this mechanism with an oscillator strength of $\sim 10^{-8}$ due to the crystal field selection rules incorporating the admixture of other states into the initial and terminal levels. It is therefore considered that the use of eqs 9a and 9b are justified since the Eu^{3+} site symmetry is C_1 in the present case. The contribution of vibronic structure to the intensity of an electronic transition is of paramount importance for high-symmetry systems,[58] but for Eu^{3+} ions in organometallic systems, most of the spectral intensity arises from pure electronic transitions. Hence, for this reason, in our largely order-of-magnitude calculations, and to avoid unnecessary complication, we do not consider vibronic intensity contributions to spectra. Additionally, we do not consider contributions from magnetic dipole transitions.

RESULTS AND DISCUSSION

Structure, Frontier Orbitals, and Calculated Spectra of $\mathbf{Eu(TTA)_3(H_2O)_2}$. The crystal structure of $\mathbf{Eu(TTA)_3(H_2O)_2}$ was reported by White (monoclinic, $P2_1/c$, $Z = 4$)[15] and subsequently, for two further isomers (triclinic, $P\bar{1}$, $Z = 2$) by Vallet and co-workers.[14] The structures are overlaid in Figure 1c, and the reader is referred to the detailed comparison given by Vallet et al. In each case, the site symmetry of the Eu^{3+} ion is C_1 and the coordination number is 8, including two aqua ligands. The FT-IR spectra of the $\mathbf{Ln(TTA)_3(H_2O)_2}$ complexes are shown in Figure 1d. The FT-IR spectrum is a good identification method, and we have compared our spectra with those previously published and with DFT calculation in Table S1.[24,25,59] We modeled the structure using the ORCA 4.2.1 program,[29,30] either in the gas phase or in toluene (employing the CPCM),[41] and the nearest-neighbor bond distances are listed in Table S2, in comparison with those from the crystal structures. The common statistic is the longer distance for Eu–O_w bonds.

Singlet Energy and Oscillator Strength. Our TD-DFT calculations in the gas phase or toluene solution indicate the ultraviolet peak maximum of $\mathbf{Eu(TTA)_3(H_2O)_2}$ at ~295 nm, Figure 1e, with the frontier orbitals from the gas-phase calculation shown in Figure 1f. The CASSCF-NEVPT2 calculation using a (6,6) active space indicates a longer wavelength, 347 nm. We envisage that after ultraviolet excitation, rapid intersystem crossing occurs from the higher singlet states to the lowest one, which then can undergo intersystem crossing and/or direct ET to Eu^{3+}. The transfer occurs from the S_1–S_0 zero phonon line (ZPL) energy, and its detailed identification and energy are discussed in the Supporting Information (SI), Section S3. In conclusion, for $\mathbf{Eu(TTA)_3(H_2O)_2}$, we take the zero phonon line energy of the lowest singlet state at 25 410 cm^{-1} (394 nm) and the oscillator strength from 0.005 up to a maximum value of 0.05. We only consider energy transfer to Eu^{3+} levels below this energy, which are above or coincident with the $^5D_0$ luminescent state. Table S3 lists the Eu^{3+} SLJ multiplet energy levels of several Eu^{3+} systems and shows that in the present ET process, Eu^{3+} could be excited to the ^5D_J ($J = 0$–3) and $^5L_6$ levels, which lie below S_1 in energy.

Triplet Energy and Oscillator Strength. Malta et al.[22] noted that the phosphorescence emission band in $\mathbf{Gd(TTA)_3(H_2O)_2}$ is not observed in $\mathbf{Eu(TTA)_3(H_2O)_2}$ and concluded that the ET from the lowest triplet state of the TTA ligand to Eu^{3+} is efficient. Other scenarios could be that the triplet level is bypassed and/or energy transfer also occurs from the singlet state. We have measured the low-temperature solid state (Figure 2a,b) and frozen-solution (Figure 2c) phosphorescence spectra of $\mathbf{Ln(TTA)_3(H_2O)_2}$ (Ln = La, Gd). The spectrum of $\mathbf{La(TTA)_3(H_2O)_2}$ solid has a strong 0–0 line at 534.7 nm (18 701 cm^{-1}) with the dominant progression frequency of 1349 cm^{-1}, corresponding to the unresolved band comprising the antisymmetric C–F stretch and the thiophene ring stretch. The corresponding Gd^{3+} complex, Figure 2b, has a spectrum similar to that previously reported,[23] but we assign the zero phonon line to the prominent peak at 508.5 nm (19 666 cm^{-1}), with the progression frequency of 1350 ± 4 cm^{-1}. The difference in zero phonon line energies for Ln = Gd, La is 965 cm^{-1}, and from this, we estimate the triplet state energy of $\mathbf{Eu(TTA)_3(H_2O)_2}$ at ~19 530 cm^{-1} (512 nm). The spectrum of $\mathbf{Gd(TTA)_3(H_2O)_2}$ in toluene at 77 K, Figure 2c, shows a blueshift of the phosphorescence from that in Figure 2b, in addition to the observation of singlet emission.

We have found that due to the magnetic/exchange properties of Gd^{3+}, the complexes generally have short phosphorescence lifetimes. Hence, to estimate the (unquenched) triplet state lifetime for $\mathbf{Eu(TTA)_3(H_2O)_2}$, we prefer to use the lifetime for the analogous La complex, which we measured as 0.2 s at 77 K in the solid state. This value is consistent with the reported

https://doi.org/10.1021/acs.jpca.2c03965
J. Phys. Chem. A 2022, 126, 7418–7431

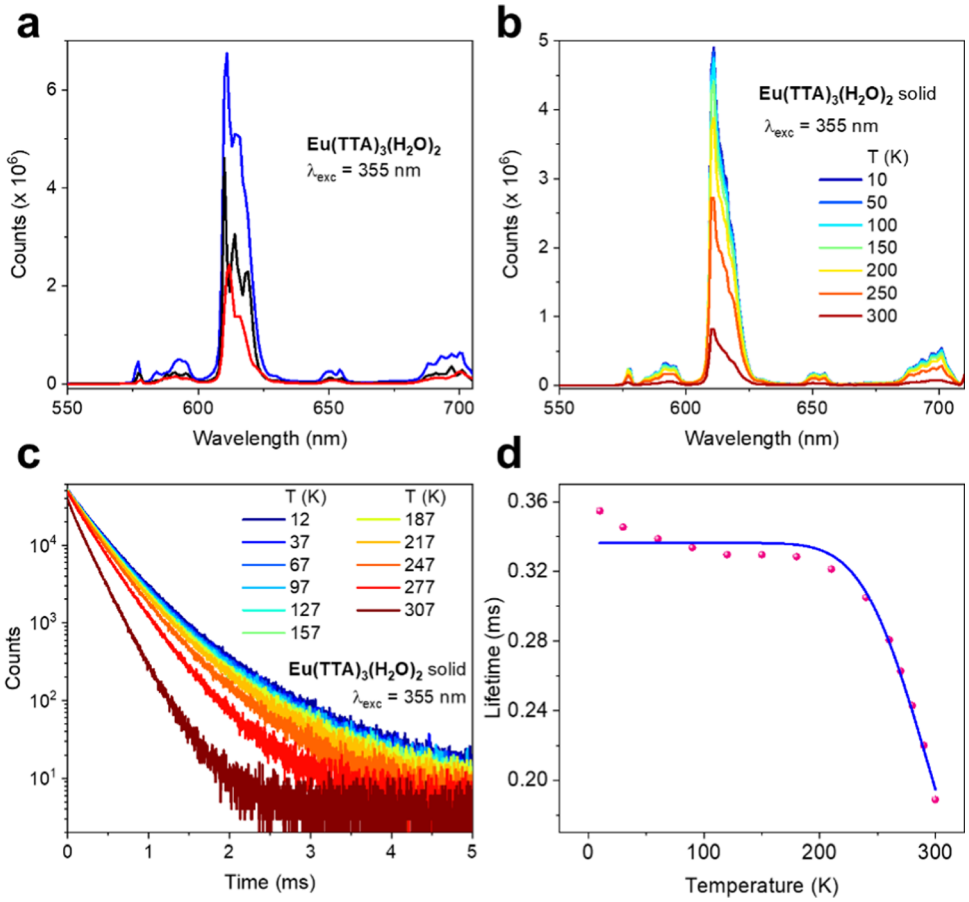

Figure 3. (a) 355 nm Excited room-temperature emission spectra of $\mathbf{Eu(TTA)_3(H_2O)_2}$: blue and black, solid, at different resolution in two instruments; red in toluene solution. The relative intensities are arbitrary for clarity of observation. (b) Temperature dependence of solid-state $\mathbf{Eu(TTA)_3(H_2O)_2}$ emission from 10 to 300 K. (c) Measured $^5D_0$ luminescence decay curves of solid $\mathbf{Eu(TTA)_3(H_2O)_2}$ at different temperatures and (d) data plot of monoexponential lifetime versus temperature. The blue line follows $y = 1/(A + B^* \exp(-C/0.695 \times x))$, with $A = 2972 \pm 26$, $B = (8.1 \pm 8.6) \times 10^6$, and $C = 1716 \pm 211$. The fit shows that other factors may be involved at lower temperatures ($R_{adj}^2 = 0.9758$).

phosphorescence lifetimes of other lanthanum complexes.[60] However, the magnitude represents the lowest value for the radiative lifetime, and using eq 1, it gives the highest value for the T_1-S_0 transition oscillator strength, $P_{if} \sim 6.53 \times 10^{-9}$.

Europium Emission Spectrum and Its Temperature Dependence. The room-temperature[22] and 77 K[23] luminescence spectra of $\mathbf{Eu(TTA)_3(H_2O)_2}$ have previously been published and assigned. We note, in Figure 3a, that the room temperature spectra differ for the solid state and toluene solution, indicating a different coordination environment for Eu^{3+}, presumably due to the loss of water in toluene solution.

Many publications employing the model of Malta have included contributions to ET rates from $^7F_1$ because at room temperature, the occupation of this *J*-multiplet is appreciable. From emission spectra, the $^7F_1$ crystal field levels of $\mathbf{Eu(TTA)_3(H_2O)_2}$ are located at 288, 358, and 493 cm^{-1}[23] so that the room temperature population ratio $^7F_1/^7F_0$ is estimated as 0.48 from the barycenter of 380 cm^{-1}.

The participation of the $^7F_1$ *J*-multiplet in facilitating ET from an antenna to Eu^{3+} has been invoked in the literature[1,21,28] because the SLJ selection rules forbid transfer involving $^7F_0$. The argument is that at room temperature, where the population of $^7F_1$ has been taken as 0.33, for example, in ref 1, it can act as an effective receiving state. Theoretically, the temperature dependence of Eu^{3+} $^5D_0$ population is weak because multiphonon relaxation to the next-lowest level, $^7F_6$, involves the energy gap of ~12 020 cm^{-1}, which is spanned by many phonons. Hence, if $^7F_1$ is dominant in participating in the ET process, one would expect an increase in Eu^{3+} emission intensity with temperature. Figure 3b shows that, unless other factors are involved, this is not the case, and that the emission intensity shows a progressive decrease with increasing temperature. The decay of $^5D_0$ at different temperatures is shown in Figure 3c, and the curves were fitted by monoexponential functions to give lifetimes in the region of 0.3 ms, which are plotted against temperature in Figure 3d and fitted by a single barrier model. The fit gives an activation energy of 1716 ± 211 cm^{-1}, which is consistent with the 1749 cm^{-1} gap between $^5D_0$ and $^5D_1$ in $\mathbf{Eu(TTA)_3(H_2O)_2}$.

Oscillator Strengths of Eu^{3+} Transitions. The europium ion transitions are very weak in intensity. Some transitions are observed in solid $\mathbf{Eu(TTA)_3(H_2O)_2}$, as marked in Figure S2, but they are not evident in toluene solution in the same figure. We have measured the oscillator strengths by absorption spectroscopy using eq 5 for data from $\mathbf{Eu(TTA)_3(H_2O)_2}$ in toluene solution and also aqueous $\mathbf{EuCl_3}$. The results are listed in Table S4 together with values from other studies.

Magnitudes of Spectral Overlap Integrals. The integral in eqs 9a, 9b, and 10 is termed the spectral overlap integral. In units of energy^{-1}, it measures the overlap of the emission band of the donor moiety with the absorption band of the acceptor. Each band is normalized to unit area. In the present case, the emission from the singlet or triplet state is very broad compared with the

https://doi.org/10.1021/acs.jpca.2c03965
J. Phys. Chem. A 2022, 126, 7418−7431

sharp intra-4f^6 absorption transitions. The SI, Section S5, gives an example of the calculation of this integral by representing the absorption and emission bands by Gaussians (Figure S4). The value was directly calculated using Maple 2021 software.[51] Alternatively, the value was calculated by summation of the intervals in the data columns,[61] and the answer was in good agreement (Section S5). We have therefore employed this summation method in the present study to calculate spectral overlap integrals (Table 1). Note that the spectral overlap integral does not represent the area bounded under the donor and acceptor curves (Figure S5), which gives a much smaller answer.

Table 1. Calculated Spectral Overlap Integrals for Various Scenarios

system[a]	transitions	SO (eV^{-1})	Figures
GdTTA phos + EuTTA abs	$T_1 \rightarrow S_0$, $^7F_0 \rightarrow {}^5D_1$	2.324	
GdTTA phos + $EuCl_3$ abs	$T_1 \rightarrow S_0$, $^7F_0 \rightarrow {}^5D_1$	2.254	4a
GdTTA phos + EuTTA em	$T_1 \rightarrow S_0$, $^5D_0 \rightarrow {}^7F_0$	1.141	4b
GdTTA phos + EuTTA em	$T_1 \rightarrow S_0$, $^5D_0 \rightarrow {}^7F_0$	1.279	S6a
GdTTA em + EuTTA abs	$S_1 \rightarrow S_0$, $^7F_1 \rightarrow {}^5D_1$	0.494	4c
GdTTA phos + EuTTA abs	$T_1 \rightarrow S_0$, $^7F_1 \rightarrow {}^5D_1$	2.317	4d
HTTA em + EuTTA em	$S_1 \rightarrow S_0$, $^5D_0 \rightarrow {}^7F_0$	0.232	S6b
GdTTA em + EuTTA em	$S_1 \rightarrow S_0$, $^5D_0 \rightarrow {}^7F_0$	0.197	S6c
GdTTA em + EuTTA abs	$S_1 \rightarrow S_0$, $^7F_0 \rightarrow {}^5D_1$	0.550	S6d
HTTA em + $EuCl_3$ abs	$S_1 \rightarrow S_0$, $^7F_0 \rightarrow {}^5D_1$	0.619	S6e
HTTA em + $EuCl_3$ abs	$S_1 \rightarrow S_0$, $^7F_0 \rightarrow {}^5D_2$	1.754	S6f
GdTTA em + EuTTA exc	$S_1 \rightarrow S_0$, $^7F_0 \rightarrow {}^5D_2$	1.326	S6g
GdTTA em + EuTTA abs	$S_1 \rightarrow S_0$, $^7F_0 \rightarrow {}^5D_2$	1.354	S6h
GdTTA em + $EuCl_3$ abs	$S_1 \rightarrow S_0$, $^7F_0 \rightarrow {}^5D_3$	1.292	S6i
GdTTA em + $EuCl_3$ abs	$S_1 \rightarrow S_0$, $^7F_0 \rightarrow {}^5L_6$	0.172	S6j

[a]LnTTA = $\mathbf{Ln(TTA)_3(H_2O)_2}$ (Ln = Gd, Eu); phos = phosphorescence spectrum; abs = absorption spectrum; em = emission spectrum; exc excitation spectrum.

The spectral overlap integrals were calculated from normalized antenna emission and europium absorption or emission bands. The antenna triplet emission spectra were taken from solid-state $\mathbf{Gd(TTA)_3(H_2O)_2}$ phosphorescence since the energy is expected to be nearer to that of $\mathbf{Eu(TTA)_3(H_2O)_2}$, rather than that of the La^{3+} complex. Singlet emission spectra were taken from **HTTA** and $\mathbf{Gd(TTA)_3(H_2O)_2}$. The Eu^{3+} data were taken from the room-temperature absorption spectra of aqueous $\mathbf{EuCl_3{\cdot}6H_2O}$ and solid-state and toluene-dissolved $\mathbf{Eu(TTA)_3(H_2O)_2}$, except for the $^5D_0-{}^7F_0$ transition, which was taken from emission spectra. The calculated values do not vary much for different combinations of the above for the same overlap, showing that the assumption is reasonable, and a selection of the resulting graphs is displayed in Figures 4 and S6. In fact, the spectral overlap integrals are all small, in the narrow range of 0.17 to 2.3 eV^{-1} (column 3, Table 1).

Calculated Energy Transfer Rates: Electric Dipole–Electric Dipole Mechanism. Table 2 summarizes the calculated ET rates using eq 9b. The transfer rates from the antenna triplet state to Eu^{3+} by this mechanism are negligible. The dominant transfer from the singlet state occurs to $^5D_2$ and $^5L_6$, although the back-transfer is appreciable for the latter. The maximum total ED–ED transfer rate involving the $^7F_0$ acceptor state is 5.1×10^7 s^{-1}, which is insufficient to quench the singlet emission. The S_1-T_1 intersystem crossing rate has been estimated to be typically in the order of 10^8 s^{-1},[12] so that this process should dominate ED–ED ET.

The appreciable population of $^7F_1$ at room temperature leads to its participation in the ET processes. Two values are listed for the oscillator strength of the ED-allowed transition $^7F_1 \rightarrow {}^5D_1$ in Table 2, taken from Table S4. The spectral overlaps are displayed for the ligand singlet and triplet transitions involving $^7F_1$ at room temperature in Figure 4c,d, respectively, and the singlet channel is much faster (Table 2) for the ED–ED mechanism. Processes involving $^7F_1 \rightarrow {}^5D_0$ (Figure S6k,l) are not considered here because the ED intensity of this transition is very weak.

Electric Dipole–Electric Quadrupole (ED–EQ) ET Mechanism. The antenna singlet and triplet transitions may follow orbitally allowed ED transitions. Besides forced ED pure electronic transitions and vibronically allowed ED transitions, some transitions of Ln^{3+} may be EQ allowed. However, the spectral intensity of such transitions is very weak. By contrast, relative to ED–ED ET, the ED–EQ ET mechanism may occur, for *fully allowed* ED and EQ transitions, respectively, with the ratio about $(a_0/R)^2$,[52,54] where a_0 is the Bohr radius ($5.291772...\times 10^{-11}$ m) and R is the donor–acceptor separation, as above. For $R \sim 4.5$ Å, this ratio is 0.014, so ED–ED ET is more important. However, the $4f^N - 4f^N$ transitions of Ln^{3+} are usually not first-order ED-allowed and are rather weaker. Taking the $^7F_0 \rightarrow {}^5D_2$ transition as an example because it is the most intense EQ allowed transition considered herein, eq 14 gives the ratio $P(\text{ED–EQ})/P(\text{ED–ED})$ of 73 so that the ED–EQ ET mechanism in this case can give a rate up to $\sim 3.0 \times 10^9$ s^{-1}. The use of eq 12b (with the oscillator strength of the EQ acceptor transition $^7F_0 \rightarrow {}^5D_2$ (6.7×10^{-12})[55] inserted into eq 11b) gives the result 3.9×10^8 s^{-1}, which is similar to the decay rate of $S_1 \rightarrow S_0$.

In summary, the combined ED–EQ and ED–ED rates from the S_1 state can therefore account for the quenching of singlet emission. The ET contributions from the triplet state to Eu^{3+} by the above mechanisms are very small, leading to its common description of "Dexter ET".

Rate Equation Approach. We apply an independent systems model to calculate the energy transfer rate to Eu^{3+} in $\mathbf{Eu(TTA)_3(H_2O)_2}$. This means that the overall metal–ligand transitions are considered independently and concurrently so that sensible ground-state populations are conserved. Seven levels are included. The antenna levels are S_1, T_1, and S_0. Other levels such as T_n were found to be of minor importance here. The Eu^{3+} levels are labeled DJ that include $^5L_6$, $^5D_3$, and $^5D_2$ combined; $^5D_1$, $^5D_0$, and $^7F_0$. The latter comprises $^7F_0$ and $^7F_1$ for simplicity here, but we have also performed calculations using separate levels. However, we have taken into account that the occupations of $^7F_0$ and $^7F_1$ are about 0.6 and 0.4 at room temperature, but 1.0 and 0.0, respectively, at 10 K. The rate constants are listed in Table 3. From the above temperature dependence of $^5D_0$ lifetime, we are confident that a charge transfer state is not involved in the energy transfer processes. The relevant experimental data for $\mathbf{Eu(TTA)_3(H_2O)_2}$ have been previously published (Figure 5).[8]

The rate equations considered are as follows:

https://doi.org/10.1021/acs.jpca.2c03965
J. Phys. Chem. A 2022, 126, 7418–7431

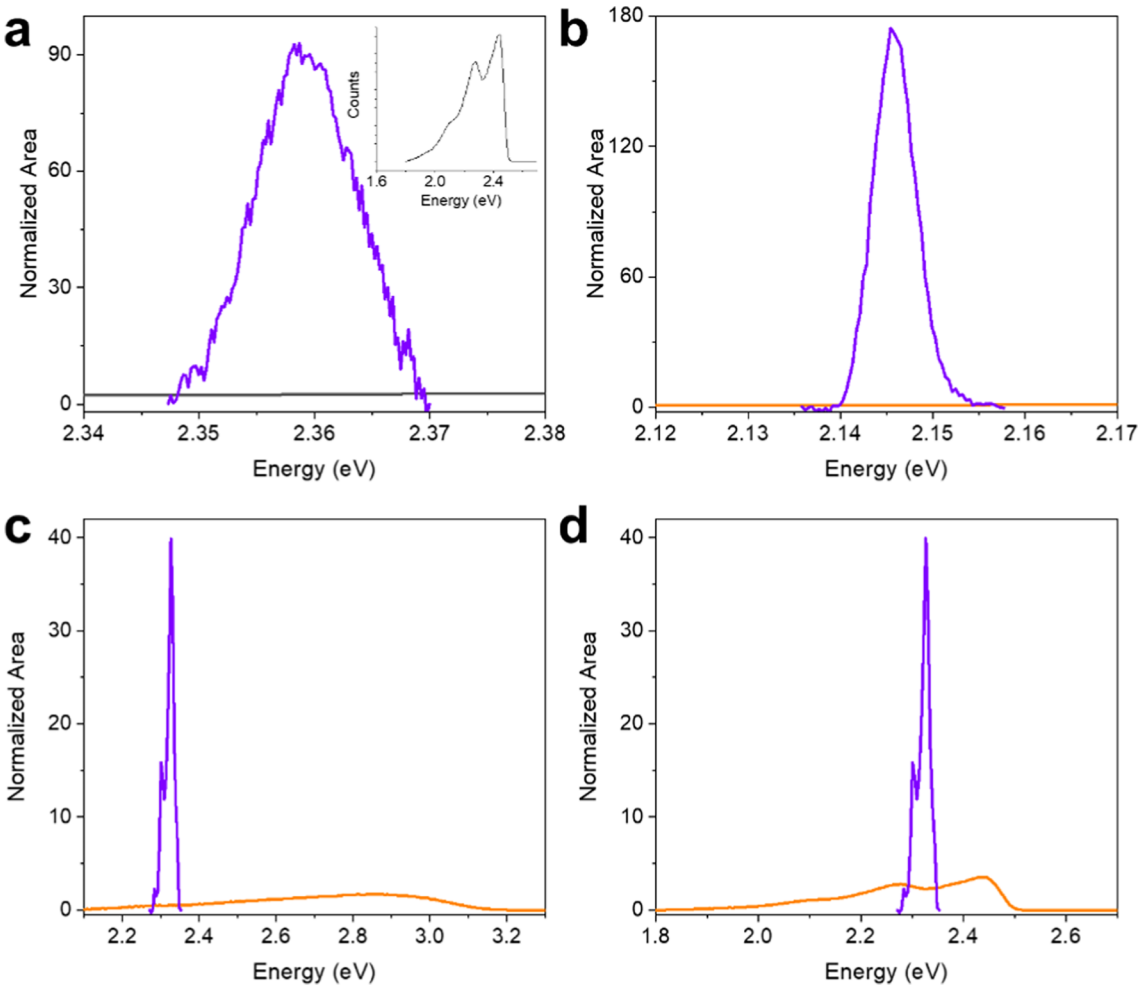

Figure 4. Examples of spectral overlap of antenna emission bands and europium absorption bands, both normalized to unity. Spectra are from this work. (a) $\mathbf{Gd(TTA)_3(H_2O)_2}$ solid-state phosphorescence spectrum (inset) and $\mathbf{EuCl_3{\cdot}6H_2O}$ aqueous room-temperature absorption spectrum; (b) $\mathbf{Gd(TTA)_3(H_2O)_2}$ solid-state phosphorescence spectrum and 10 μM $\mathbf{Eu(TTA)_3(H_2O)_2}$ in toluene room-temperature emission spectrum. (c) $\mathbf{Gd(TTA)_3(H_2O)_2}$ solid-state singlet emission and $\mathbf{Eu(TTA)_3(H_2O)_2}$ solid-state room-temperature absorption spectrum. (d) $\mathbf{Gd(TTA)_3(H_2O)_2}$ solid-state phosphorescence spectrum and $\mathbf{Eu(TTA)_3(H_2O)_2}$ solid-state room-temperature absorption spectrum.

1. $d[S_1]/dt = Q - (f + b)*[S_1] - (g + m + k)*[S_1]*[^7F_0]$
2. $d[T_1]/dt = f*[S_1] - (n + p)*[T_1]*[^7F_0] - a[T_1]$
3. $d[DJ]/dt = g*[S_1]*[^7F_0] - s*[DJ]$
4. $d[^5D_1]/dt = s*[DJ] - (d + u)*[^5D_1] + n*[T_1]*[^7F_0] + k*[S_1]*[^7F_0]$
5. $d[^5D_0]/dt = -c*[^5D_0] + d*[^5D_1] + m*[S_1]*[^7F_0] + p*[T_1]*[^7F_0]$
6. $d[^7F_0]/dt = c*[^5D_0] + u*[^5D_1] - (m + g + k)*[^7F_0]*[S_1] - (p + n)*[T_1]*[^7F_0]$
7. $d[S_0]/dt = -Q + a*[T_1] + b*[S_1] + (n + p)*[T_1]*[^7F_0] + (g + k + m)*[S_1]*[^7F_0]$

These equations were solved in Maple 2021[51] by the Rosenbrock method with the initial concentrations of $[S_0] = 1$, $[^7F_0] = 1$, and others zero. The concentrations at 5 ns were determined, and these were employed in the further calculation with zero excitation ($Q = 0$). The rationale for parameter values is given in SI, Section S7. The values are representative, and we have not made an effort to fine-tune them to simulate experimental data.

The first calculations assumed, as often done, that the energy transfer to Eu^{3+} arises solely from the triplet state. In this case, the rate parameters k, m, and g were set to zero. The 300 K risetime of $^5D_1$ from Figure 4 in ref 8 is ~30 ns, which infers an ET rate (parameter n) of 3.33×10^7 s^{-1} if the transfer is only from T_1. The 300 K decay time of $^5D_1$ is 0.4 μs.[8] Using the other illustrative values in Table 3, for this zero singlet ET scenario (Szero), the calculated concentrations of the different states are plotted against time in Figure S7 (black lines) and subsequently fitted by mono- or biexponential functions (red lines). The calculated risetime of $^5D_1$ was found to be 20 ns, which is the same as the triplet decay time. To simulate 10 K conditions, the calculation was repeated with the contributions to energy transfer from $^7F_1$ omitted, Figure S8 (Table 3, column 4, also with the $^5D_1$ and $^5D_0$ lifetimes adjusted for their temperature dependence). Again, the $^5D_1$ risetime equals the triplet decay time, but it only increases to 23 ns, far from the experimental value ~70 ns as in Figure 4b, ref 8. We therefore consider that other parameters would need to change to achieve a longer

https://doi.org/10.1021/acs.jpca.2c03965
J. Phys. Chem. A 2022, 126, 7418−7431

Table 2. Electric Dipole−Electric Dipole Energy Transfer Rates for $Eu(TTA)_3(H_2O)_2$[a]

ET transition[b]	P_D (ED)	P_A (ED)	SO (eV^{-1})	$\bar{\nu}_{av}$ (cm^{-1})	W^f_{ET} (s^{-1})	W^b_{ET} (s^{-1})
$T_1-{}^5D_0$	6.53E-9	1.66E-10	1.21	18417	0.001	2.2E-8
		7.9E-8			0.491	1.1E-5
$T_1-{}^5D_1$	6.53E-9	7.2E-10	2.29	19291	0.008	7.7E-4
$S_1-{}^5D_0$	0.05	1.66E-10	0.197	21357	956	9.9E-15
		7.9E-8			4.6E5	4.7E-12
$S_1-{}^5D_1$	0.05	7.2E-10	0.551	22231	1.071E4	1.6E-9
$S_1-{}^5D_2$	0.05	1.32E-6	1.335	23481	4.26E7	0.35
		1.36E-8			4.39E5	3.63E-3
$S_1-{}^5D_3$	0.05	2.74E-8	1.292	24891	7.62E5	5.1E3
$S_1-{}^5L_6$	0.05	1.82E-6	0.172	25278	6.53E6	1.83E6
$S_1-({}^7F_1-{}^5D_1)$	0.05	6.1E-8	0.494	22086	8.24E5	9.7E-9
		8.5E-6			1.15E8	1.4E-6
$T_1-({}^7F_1-{}^5D_1)$	6.53E-9	6.1E-8	2.317	19146	0.67	0.02
		8.5E-6			94	2.8

[a] P_D and P_A are the donor and acceptor ED oscillator strengths. SO is the spectral overlap integral and $\bar{\nu}_{av}$ is the donor−acceptor average energy. W^f_{ET} and W^b_{ET} are, respectively, the forward and backward rates according to the Boltzmann equation. The distance R in eq 9b was fixed at 4.5 Å as discussed above.[21] Only the ED contribution to the oscillator strength of ${}^7F_0 \rightarrow {}^5D_1$ has been considered. The ED-MD (MD = magnetic dipole) ET rate is zero for a centrosymmetric system[62] and is expected to be small in other cases.[54] The oscillator strength of $S_1 \rightarrow S_0$ is given as 0.05, which is probably 1 order of magnitude too high (SI, Section S3), and if so, the calculated W_{ET} then needs to be reduced by a factor of 10. Alternative oscillator strengths are given for ${}^7F_0 \rightarrow {}^5D_0$ and the hypersensitive ${}^7F_0 \rightarrow {}^5D_2$ transition, according to the data in Table S4. [b] The initial Eu^{3+} state is ${}^7F_0$ unless indicated, and the final antenna state is S_0.

Table 3. Rate Constants, Their Meanings, and Values Adopted in the Calculations

rate constant[a]	meaning	value 300 K	value 10 K
Q	$S_0 \rightarrow S_1$ excitation	10	10
a	$T_1 \rightarrow S_0$ nonradiative and radiative decay	1E6	1E2
b	$S_1 \rightarrow S_0$ fluorescence decay	3E8	3E8
f	$S_1 \rightarrow T_1$ intersystem crossing	1E9	1E9
c	${}^5D_0 \rightarrow {}^7F_J$ luminescence	5000	3906
g	$S_1 \rightarrow S_0\ {}^7F_0 \rightarrow D_J$ energy transfer	1E9	1E9
k	$S_1 \rightarrow S_0\ {}^7F_0 \rightarrow {}^5D_1$ energy transfer	1.1E8	1.1E4
m	$S_1 \rightarrow S_0\ {}^7F_0 \rightarrow {}^5D_0$ energy transfer	1.17E6	4.6E5
n	$T_1 \rightarrow S_0\ {}^7F_0 \rightarrow {}^5D_1$ energy transfer	3.33E7	2.84E7
p	$T_1 \rightarrow S_0\ F_0 \rightarrow {}^5D_0$ energy transfer	1.5E7	1.5E7
s	$DJ \rightarrow {}^5D_1$ internal conversion	1E8	1E8
d	${}^5D_1 \rightarrow {}^5D_0$ internal conversion	2.5E6	2.5E5
u	${}^5D_1 \rightarrow {}^7F_J$ luminescence	1E4	1.5E5

[a] Unit s^{-1} or $mol^{-1}\ s^{-1}$.

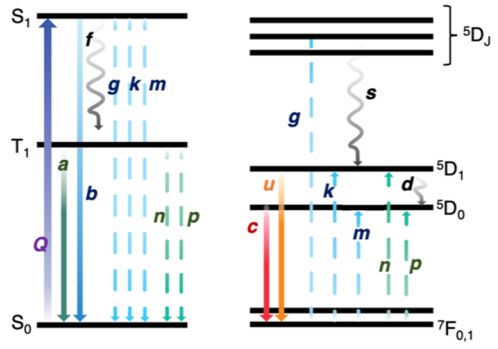

Figure 5. Rate constants in the independent systems model.

risetime but reducing the intersystem crossing rate (f) by a factor of 10 from 300 to 10 K has little effect upon the ${}^5D_1$ risetime (Figure S9) and increasing parameter a to $10^6\ s^{-1}$ has no effect (Figure S10).

An alternative model involves ET from solely the singlet state (the Tzero model), as displayed in Figure S11 for 300 K. Again, there is a ${}^5D_1$ risetime in the ns range, in this case 10 ns. By comparison with the previous Szero model, this leads to the conclusion that the experimental observation of a ns risetime for ${}^5D_1$ does not enable one to judge if the ET route involves singlet or triplet ET, let alone the operating mechanism, as has often been done. Taking into account the changes in ${}^5D_0$ and ${}^5D_1$ lifetimes and the absence of ET involving ${}^7F_1$, the 10 K profiles are shown in Figure S12 and the ${}^5D_1$ risetime does not differ from that at room temperature. However, if the internal conversion rate (parameter s) is reduced by a factor of 10 as in Figure S13, which is reasonable for such a temperature change, the ${}^5D_1$ risetime increases up to 102 ns. This could be a signature of mainly singlet energy transfer.

The two above models, Szero and Tzero, show that the feeder state, T_1 or ${}^5D_2$, determines the ${}^5D_1$ risetime and that while, from 300 to 10 K, a 10-fold change of ${}^5D_2-{}^5D_1$ internal conversion rate is reasonable and produces a longer risetime, the change of rate involving T_1 only slightly modifies the risetime. Hence, in principle, we can distinguish singlet or triplet ET by monitoring the change in ${}^5D_1$ risetime with temperature.

Figure 6 displays the ET scenario from ligand to Eu^{3+} at 300 K with combined singlet and triplet energy transfer as in columns 3 and 7, Table 3: 96% from S_1 and 4% from T_1. Remember that the exchange contribution to T_1 is not known, but we can put an upper limit on it from the ${}^5D_1$ risetime.

The ${}^5D_1$ risetime is intermediate (14 ns) between the Szero and Tzero models. The profile for ${}^7F_0$ is interesting because it displays both the nanosecond decrease (as in Szero) and the long risetime as in Tzero. The latter is determined by ${}^5D_0$ decay, whereas the former is the same as the T_1 decay time and the S_0 risetime. Monitoring the population of ${}^7F_0$ (although difficult) may therefore be fruitful when considering energy transfer mechanisms.

Using the parameters in Table 3, columns 4 and 8, to simulate the 10 K kinetics (Figure S14), the ${}^5D_1$ risetime is intermediate between the decay times of ${}^5D_2$ (DJ) and T_1 but is similar to the

https://doi.org/10.1021/acs.jpca.2c03965
J. Phys. Chem. A 2022, 126, 7418−7431

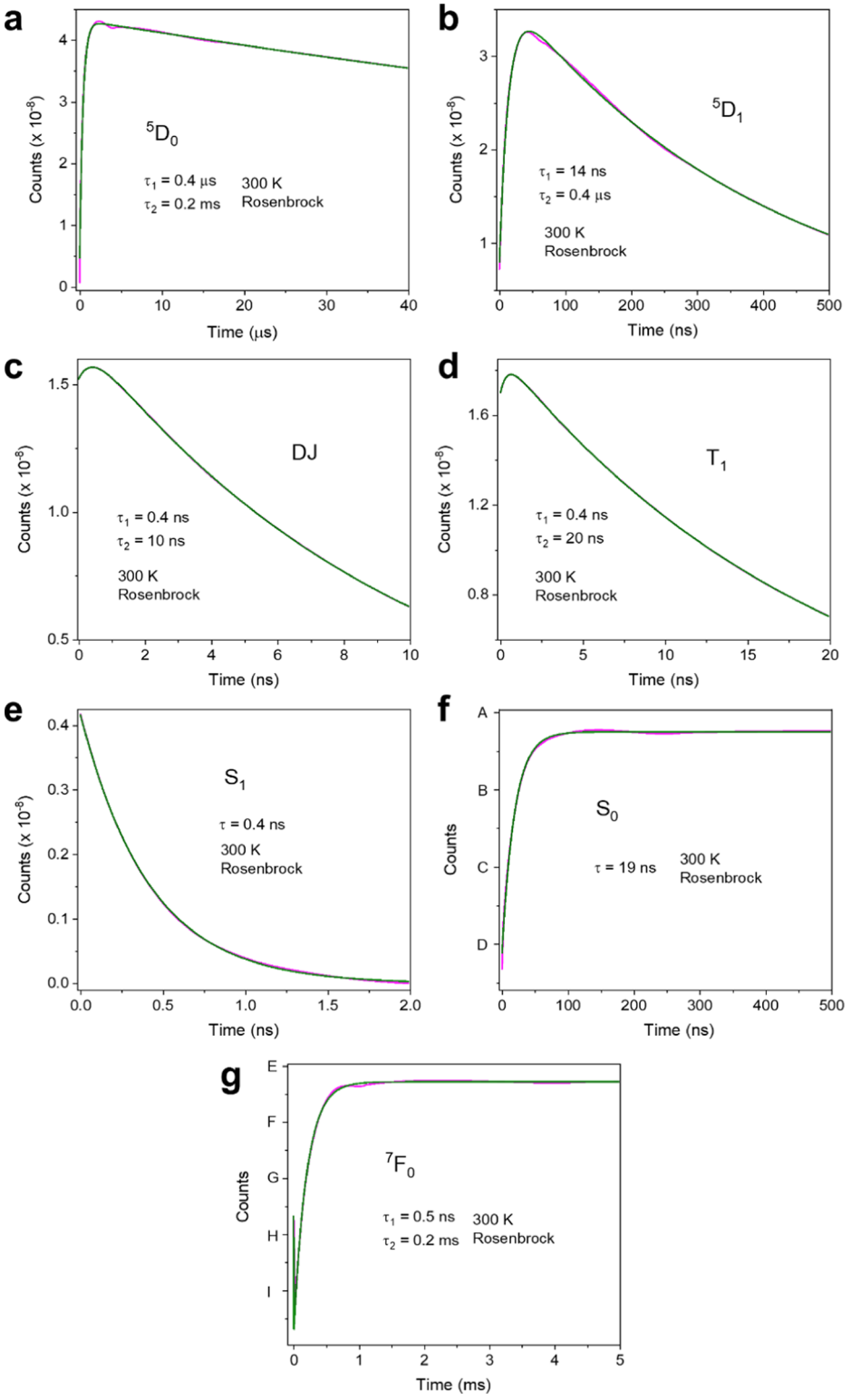

Figure 6. Calculated (black lines) 300 K time profiles of levels using the Rosenbrock method, following a 5 ns pulse. (a) $^5D_0$; (b) $^5D_1$; (c) DJ; (d) T_1; (e) S_1; (f) S_0; (g) $^7F_0$. The parameters are in columns 3 and 7 of Table 3. The red lines are fits to the calculated data using mono- or biexponential functions, with the fitted lifetimes as indicated. In S_0 and F_0: A 1.000000002; B 0.9999999948; C 0.999999988; D 0.9999999811; E 1.000000003; F 0.999999993; G 0.9999999835; H 0.9999999739; I 0.9999999643.

room temperature value. However, taking into account the slowing of the $^5D_2$–$^5D_1$ internal conversion rate by an order of magnitude from 300 to 10 K (with rate constant s changed in Table 3, column 8, to 10^7 s^{-1}, Figure 7), the $^5D_1$ risetime becomes much longer.

We summarize the results from the model as follows:

1. The maximum total ET rate from the ligand singlet state to the acceptor $^7F_0$ state *via* the ED–ED mechanism is of the order 10^7 s^{-1}. The rate involving the acceptor state $^7F_1$ is up to the order 10^8 s^{-1}. The intensity of Eu^{3+} emission

https://doi.org/10.1021/acs.jpca.2c03965
J. Phys. Chem. A 2022, 126, 7418–7431

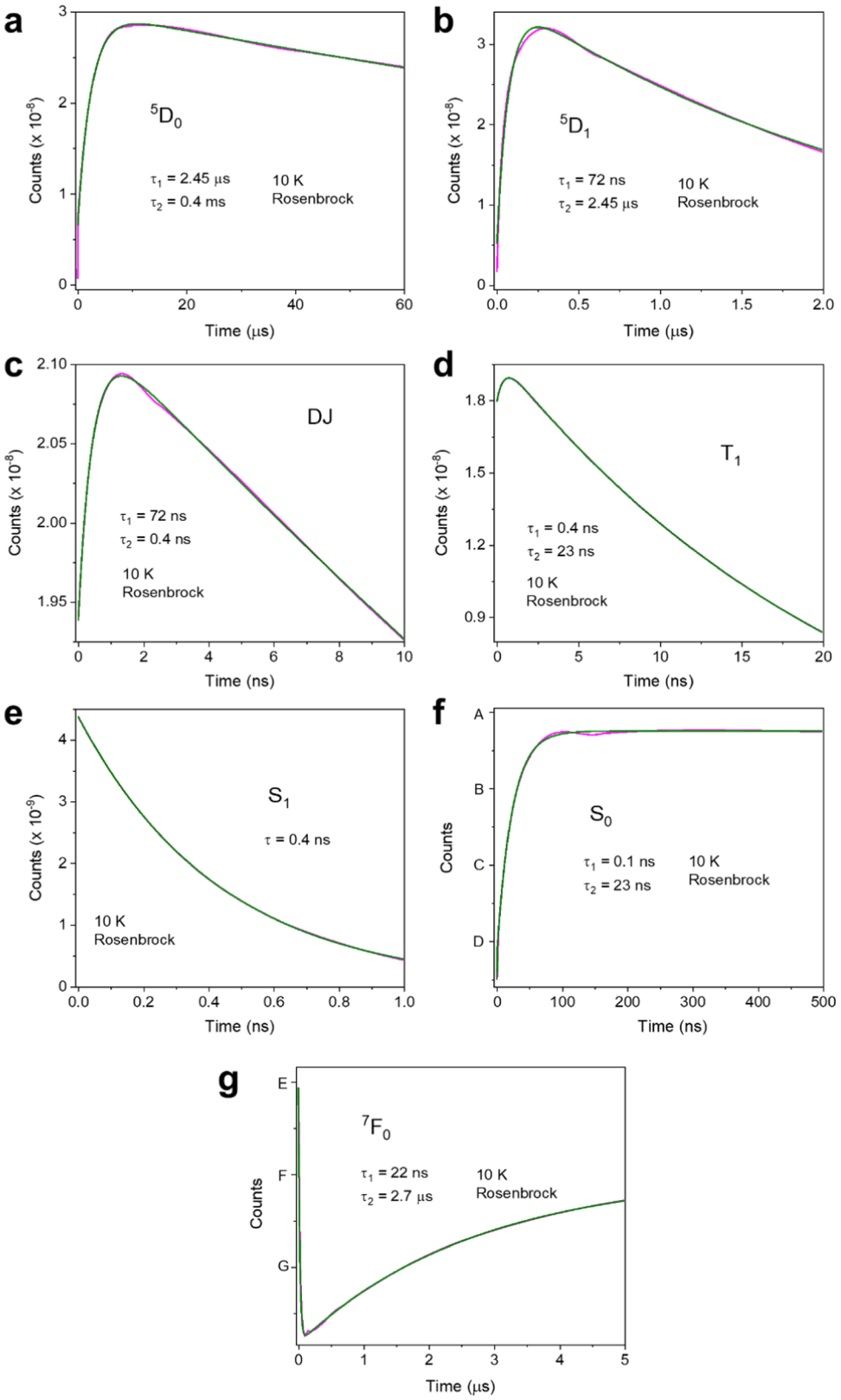

Figure 7. Calculated 10 K time profiles of levels using the Rosenbrock method, following a 5 ns pulse (black lines). (a) $^5D_0$; (b) $^5D_1$; (c) DJ; (d) T_1; (e) S_1; (f) S_0; (g) $^7F_0$. The parameters are in columns 4 and 8 of Table 3, with the exception that $s = 10^7$ s^{-1}. The red lines are fits to the calculated data using mono- or biexponential functions, with the fitted lifetimes as indicated. In S_0 and F_0: A 1.000000002; B 0.9999999948; C 0.999999988; D 0.9999999811; E 0.9999999788; F 0.9999999708; G 0.9999999629.

decreases with increasing temperature despite an increasing ET rate involving the $^7F_1$ acceptor state. The maximum rate for ED−EQ transfer (10^8–10^9 s^{-1}) is sufficient to quench the singlet emission. We are presently

https://doi.org/10.1021/acs.jpca.2c03965
J. Phys. Chem. A 2022, 126, 7418−7431

unable to calculate the ET rate for exchange interaction but our calculations of the $^5D_1$ risetime indicate a value in the range of 10^7 s^{-1}.

2. The ET rate from the triplet state by ED−ED and ED−EQ mechanisms is very weak but is still enough to quench the long lifetime triplet emission.

3. The observation of a nanosecond risetime for $^5D_1$ does not enable distinction of triplet or singlet ET, let alone the mechanism. The $^5D_1$ risetime may be contributed by several processes.

4. Following the $^5D_1$ risetime as a function of temperature and using the temporal profile of $^7F_0$ may provide useful information concerning the energy transfer route.

CONCLUSIONS

We have employed the Dexter formalism[54] to investigate the ET mechanisms and rates from an antenna to a lanthanide ion, with the complex $\mathbf{Eu(TTA)_3(H_2O)_2}$ as a case study. This compound may not have been a good choice in view of its rapid decomposition in moist air, but our spectra are consistent with those of previous studies. Considerable differences exist between the spectra for the complex in the solid state and in dilute solution. These arise from the enormous concentration factor in the solid state and merit further study. The use of the experimental data for oscillator strengths and spectral overlap enables ET rates to be calculated for ED−ED and ED−EQ ET. As previously shown,[61] the Förster and Dexter formalisms are the same for ED−ED transfer, with the exception of local field effects. The independent systems model is successful in reproducing the temporal variation of experimental data. The model can be applied on different timescales and is general for Eu^{3+} complexes except for special cases, such as the involvement of a charge transfer state, where the model can be further adapted by its inclusion. This study does show that time-gated spectroscopy together with transient absorption measurements could provide detailed information to understand the kinetics of energy transfer in Eu^{3+} complexes.

In the Supporting Information, we have commented upon the software LUMPAC and JOYSpectra, which both use the model of Malta. We consider that the use of an approximation for the exchange integral and a fixed value may not be justified. The major outstanding problem therefore lies with the calculation of exchange ET rate. Some previous reports have considered the evaluation of two-center exchange integrals, and we will study these to apply the formalism of Dexter and calculate the exchange contribution to ET.

ASSOCIATED CONTENT

Supporting Information

The Supporting Information is available free of charge at https://pubs.acs.org/doi/10.1021/acs.jpca.2c03965.

Experimental (S1); computation of molecular structure (S2); singlet energy and oscillator strength (S3); oscillator strengths (S4); spectral overlap integral (S5); spectral overlap diagrams (S6); rate equation model (S7); calculations using the model of Malta (S8); units and conversions used in this work (S9); and references (S10) (PDF)

AUTHOR INFORMATION

Corresponding Authors

Peter A. Tanner − *Department of Chemistry, Hong Kong Baptist University, Kowloon Tong, Hong Kong S.A.R., P. R. China;* orcid.org/0000-0002-4681-6203; Email: peter.a.tanner@gmail.com

Ka-Leung Wong − *Department of Chemistry, Hong Kong Baptist University, Kowloon Tong, Hong Kong S.A.R., P. R. China;* orcid.org/0000-0002-3750-5980; Email: klwong@hkbu.edu.hk

Authors

Waygen Thor − *Department of Chemistry, Hong Kong Baptist University, Kowloon Tong, Hong Kong S.A.R., P. R. China;* orcid.org/0000-0002-4366-9113

Yonghong Zhang − *State Key Laboratory of Chemistry and Utilization of Carbon Based Energy Resources, Key Laboratory of Oil and Gas Fine Chemicals, Ministry of Education & Xinjiang Uygur Autonomous Region, Urumqi Key Laboratory of Green Catalysis and Synthesis Technology, College of Chemistry, Xinjiang University, Urumqi 830017 Xinjiang, P. R. China;* orcid.org/0000-0002-7740-9408

Complete contact information is available at: https://pubs.acs.org/10.1021/acs.jpca.2c03965

Notes

The authors declare no competing financial interest.

ACKNOWLEDGMENTS

K.-L.W. acknowledges funding from the Hong Kong Research Grants Council Research Grant No. 1230020. The authors thank the Max-Planck-Institut für Chemische Energiekonversion for making available the Orca Program. This research was conducted using the resources of the High Performance Cluster Computing Center, Hong Kong Baptist University, which receives funding from the Research Grant Council, University Grant Committee of the HKSAR and Hong Kong Baptist University. The authors also thank Sci-Hub for removing barriers in the way to science. They also thank Dr. Jose Diogo de Lisboa Dutra for private discussions concerning LUMPAC and Prof. O.L. Malta and his group for correspondence. Professor Y. Y. Yeung is thanked for providing the free ion compositions of multiplet terms of some europium complexes.

REFERENCES

(1) Kasprzycka, E.; Trush, V. A.; Amirkhanov, V. M.; Jerzykiewicz, L.; Malta, O. L.; Legendziewicz, J.; Gawryszewska, P. Contribution of Energy Transfer from the Singlet State to the Sensitization of Eu^{3+} and Tb^{3+} Luminescence by Sulfonylamidophosphates. *Chem. − Eur. J.* **2017**, *23*, 1318−1330.

(2) Carlos, L. D.; Faustino, W. M.; Malta, O. L. Comment on Trivalent Europium Lifetimes in the Presence of Intramolecular Energy Transfer Processes. *J. Braz. Chem. Soc.* **2008**, *19*, 299−301.

(3) Yang, C.; Fu, L.-M.; Wang, Y.; Zhang, J.-P.; Wong, W.-T.; Ai, X.-C.; Qiao, Y.-F.; Zou, B.-S.; Gui, L.-L. A Highly Luminescent Europium Complex Showing Visible-Light-Sensitized Red Emission: Direct Observation of the Singlet Pathway. *Angew. Chem., Int. Ed.* **2004**, *43*, 5010−5013.

(4) Miyazaki, S.; Miyata, K.; Sakamoto, H.; Suzue, F.; Kitagawa, Y.; Hasegawa, Y.; Onda, K. Dual Energy Transfer Pathways from an Antenna Ligand to Lanthanide Ion in Trivalent Europium Complexes with Phosphine-Oxide Bridges. *J. Phys. Chem. A* **2020**, *124*, 6601−6606.

(5) Fu, L.-M.; Ai, X.-C.; Li, M.-Y.; Wen, X.-F.; Hao, R.; Wu, Y.-S.; Wang, Y.; Zhang, J.-P. Role of Ligand-to-Metal Charge Transfer State in

Nontriplet Photosensitization of Luminescent Europium Complex. *J. Phys. Chem. A* **2010**, *114*, 4494−4500.
(6) Mara, M. W.; Tatum, D. S.; March, A.-M.; Doumy, G.; Moore, E. G.; Raymond, K. N. Energy Transfer from Antenna Ligand to Europium(III) Followed Using Ultrafast Optical and X-Ray Spectroscopy. *J. Am. Chem. Soc.* **2019**, *141*, 11071−11081.
(7) Gawryszewska, P.; Moroz, O. V.; Trush, V. A.; Amirkhanov, V. M.; Lis, T.; Sobczyk, M.; Siczek, M. Spectroscopy and Structure of Ln^{III} Complexes with Sulfonylamidophosphate-Type Ligands as Sensitizers of Visible and Near-Infrared Luminescence. *ChemPlusChem* **2012**, *77*, 482−496.
(8) Faustino, W. M.; Nunes, L. A.; Terra, I. A. A.; Felinto, M. C. F. C.; Brito, H. F.; Malta, O. L. Measurement and Model Calculation of the Temperature Dependence of Ligand-to-Metal Energy Transfer Rates in Lanthanide Complexes. *J. Lumin.* **2013**, *137*, 269−273. Note the error in this publication: in the caption of Figure 4 (μs is written instead of ns) and the color coding in the Figure 4b needs to be reversed.
(9) Lis, S.; Elbanowski, M.; Makowska, B.; Hnatejko, Z. Energy Transfer in Solution of Lanthanide Complexes. *J. Photochem. Photobiol., A* **2002**, *150*, 233−247.
(10) Tanaka, F.; Ishibashi, T. Energy Transfer between Lanthanide Ions in Dinuclear Complexes. *J. Chem. Soc., Faraday Trans.* **1996**, *92*, 1105−1110.
(11) Wang, J.; Deng, R. Energy Transfer in Dye-Coupled Lanthanide-Doped Nanoparticles: From Design to Application. *Chem. − Asian J.* **2018**, *13*, 614−625.
(12) Carneiro Neto, A. N.; Teotonio, E. E. S.; de Sá, G. F.; Brito, H. F.; Legendziewicz, J.; Carlos, L. D.; Felinto, M. C. F. C.; Gawryszewska, P.; Moura, R. T., Jr.; Longo, R. L.et al.Modeling Intramolecular Energy Transfer in Lanthanide Chelates: A Critical Review and Recent Advances. In *Handbook on the Physics and Chemistry of Rare Earths*, Including Actinides; Elsevier, 2019; Vol. *56*, pp 55−162.
(13) Moore, E. G.; Samuel, A. P. S.; Raymond, K. N. From Antenna to Assay: Lessons Learned in Lanthanide Luminescence. *Acc. Chem. Res.* **2009**, *42*, 542−552.
(14) Vallet, V.; Fischer, A.; Szabó, Z.; Grenthe, I. The Structure and Bonding of Y, Eu, U, Am and Cm Complexes as Studied by Quantum Chemical Methods and X-Ray Crystallography. *Dalton Trans.* **2010**, *39*, 7666−7672.
(15) White, J. G. The Crystal Structure of Europium Tris[4,4,4,-trifluoro-1-(2-thienyl)-1,3-butanedione] Dihydrate. *Inorg. Chim. Acta* **1976**, *16*, 159−162.
(16) Malta, O. L. Ligand-Rare-Earth Ion Energy Transfer in Coordination Compounds. A Theoretical Approach. *J. Lumin.* **1997**, *71*, 229−236.
(17) Malta, O. L. Mechanisms of Non-Radiative Energy Transfer Involving Lanthanide Ions Revisited. *J. Non-Cryst. Solids* **2008**, *354*, 4770−4776.
(18) Malta, O. L.; Gonçalves e Silva, F. R. A Theoretical Approach to Intramolecular Energy Transfer and Emission Quantum Yields in Coordination Compounds of Rare Earth Ions. *Spectrochim. Acta, Part A* **1998**, *54*, 1593−1599.
(19) Kushida, T. Energy Transfer and Cooperative Optical Transitions in Rare-Earth Doped Inorganic Materials. I. Transition Probability Calculation. *J. Phys. Soc. Jpn.* **1973**, *34*, 1318−1326.
(20) Dutra, J. D. L.; Bispo, T. D.; Freire, R. O. LUMPAC Lanthanide Luminescence Software: Efficient and User Friendly. *J. Comput. Chem.* **2014**, *35*, 772−775.
(21) Moura, R. T., Jr.; Carneiro Neto, A. N.; Aguiar, E. C.; Santos-Jr, C. V.; de Lima, E. M.; Faustino, W. M.; Teotonio, E. E. S.; Brito, H. F.; Felinto, M. C. F. C.; Ferreira, R. A. S.; et al. JOYSpectra: A Web Platform for Luminescence of Lanthanides. *Opt. Mater.: X* **2021**, *11*, 100080.
(22) Malta, O. L.; Brito, H. F.; Menezes, J. F. S.; Gongalves e Silva, F. R.; Alves, S., Jr.; Farias, F. S., Jr.; de Andrade, A. V. M. Spectroscopic Properties of a New Light-Converting Device Eu-(Thenoyltrifluoroacetonate)$_3$2(Dibenzyl Sulfoxide). A Theoretical Analysis Based on Structural Data Obtained from A Sparkle Model. *J. Lumin.* **1997**, *75*, 255−268.
(23) Teotonio, E. E. S.; Brito, H. F.; Felinto, M. C. F. C.; Kodaira, C. A.; Malta, O. L. Luminescence Investigations on Eu(III) Thenoyltrifluoroacetonate Complexes with Amide Ligands. *J. Coord. Chem.* **2003**, *56*, 913−921.
(24) Charles, R. G.; Ohlmann, R. C. Europium thenoyltrifluoroacetonate, Preparation and Fluorescence Properties. *J. Inorg. NucI. Chem.* **1965**, *27*, 255−259.
(25) Fernandes, M.; de Zea Bermudez, V.; Sá Ferreira, R. A.; Carlos, L. D.; Charas, A.; Morgado, J.; Silva, M. M.; Smith, M. J. Highly Photostable Luminescent Poly(ε-caprolactone)siloxane Biohybrids Doped with Europium Complexes. *Chem. Mater.* **2007**, *19*, 3892−3901.
(26) Zhou, L.; Zhang, H.; Deng, R.; Li, Z.; Yu, J.; Guo, Z. Conversion Process of the Dominant Electroluminescence Mechanism in a Molecularly Doped Organic Light-Emitting Device with Only Electron Trapping. *J. Appl. Phys.* **2007**, *102*, 064504.
(27) Zucchi, G.; Murugesan, V.; Tondelier, D.; Aldakov, D.; Jeon, T.; Yang, F.; Thuéry, P.; Ephritikhine, M.; Geffroy, B. Solution, Solid State, and Film Properties of a Structurally Characterized Highly Luminescent Molecular Europium Plastic Material Excitable with Visible Light. *Inorg. Chem.* **2011**, *50*, 4851−4856.
(28) Blois, L.; Carneiro Neto, A. N.; Malta, O. L.; Brito, H. F. The Role of the Eu^{3+} $^7F_1$ Level in the Direct Sensitization of the $^5D_0$ Emitting Level through Intramolecular Energy Transfer. *J. Lumin.* **2022**, *247*, 118862.
(29) Neese, F. The ORCA Program System. *Wiley Interdiscip. Rev.: Comput. Mol. Sci.* **2012**, *2*, 73−78.
(30) Neese, F. Software Update: the ORCA Program System, Version 4.0. *Wiley Interdiscip. Rev.: Comput. Mol. Sci.* **2018**, *8*, No. e1327.
(31) Avogadro: An Open-Source Molecular Builder and Visualization Tool. Version 1.2.0. http://avogadro.cc/ (Accessed on 18 August 2022).
(32) Hanwell, M. D.; Curtis, D. E.; Lonie, D. C.; Vandermeersch, T.; Zurek, E.; Hutchison, G. R. Avogadro: An Advanced Semantic Chemical Editor, Visualization, and Analysis Platform. *J. Cheminf.* **2012**, *4*, No. 17.
(33) Allouche, A.-R. Gabedit-A Graphical User Interface for Computational Chemistry Softwares. *J. Comput. Chem.* **2011**, *32*, 174−182.
(34) (a) Perdew, J. P. Density-Functional Approximation for the Correlation Energy of the Inhomogeneous Electron Gas. *Phys. Rev. B* **1986**, *33*, 8822−8824;(b) *Erratum: Phys. Rev. B* **1986**, *34*, 7406.
(35) (a) Perdew, J. P.; Burke, K.; Ernzerhof, M. Generalized Gradient Approximation Made Simple. *Phys. Rev. Lett.* **1996**, *77*, 3865−3868;(b) *Erratum: Phys. Rev. Lett.* **1997**, *78*, 1396.
(36) Weigend, F.; Ahlrichs, R. Balanced Basis Sets of Split Valence, Triple Zeta Valence and Quadruple Zeta Valence Quality for H to Rn: Design and Assessment of Accuracy. *Phys. Chem. Chem. Phys.* **2005**, *7*, 3297−3305.
(37) Andrae, D.; Haeussermann, U.; Dolg, M.; Stoll, H.; Preuss, H. Energy-Adjusted ab Initio Pseudopotentials for the Second and Third Row Transition Elements. *Theor. Chim. Acta* **1990**, *77*, 123−144.
(38) Dolg, M.; Stoll, H.; Savin, A.; Preuss, H. Energy-Adjusted Pseudopotentials for the Rare Earth Elements. *Theor. Chim. Acta* **1989**, *75*, 173−194.
(39) Grimme, S.; Ehrlich, S.; Goerigk, L. Effect of the Damping Function in Dispersion Corrected Density Functional Theory. *J. Comput. Chem.* **2011**, *32*, 1456−1465.
(40) Grimme, S.; Antony, J.; Ehrlich, S.; Krieg, H. A Consistent and Accurate ab initio Parametrization of Density Functional Dispersion Correction (DFT-D) for the 94 Elements H-Pu. *J. Chem. Phys.* **2010**, *132*, No. 154104.
(41) Garcia-Ratés, M.; Neese, F. Efficient Implementation of the Analytical Second Derivatives of Hartree-Fock and Hybrid DFT Energies within the Framework of the Conductor-Like Polarizable Continuum Model. *J. Comput. Chem.* **2019**, *40*, 1816−1828.
(42) Angeli, C.; Cimiraglia, R.; Evangelisti, S.; Leininger, T.; Malrieu, J.-P. Introduction of *N*-electron Valence States for Multireference Perturbation Theory. *J. Chem. Phys.* **2001**, *114*, 10252−10264.

https://doi.org/10.1021/acs.jpca.2c03965
J. Phys. Chem. A 2022, 126, 7418−7431

(43) Angeli, C.; Cimiraglia, R.; Malrieu, J.-P. *N*-electron Valence State Perturbation Theory: A Fast Implementation of the Strongly Contracted Variant. *Chem. Phys. Lett.* **2001**, *350*, 297−305.
(44) Angeli, C.; Cimiraglia, R.; Malrieu, J.-P. *N*-electron Valence State Perturbation Theory: A Spinless Formulation and an Efficient Implementation of the Strongly Contracted and of the Partially Contracted Variants. *J. Chem. Phys.* **2002**, *117*, 9138−9153.
(45) Hehre, W. J.; Ditchfield, R.; Pople, J. A. Self-Consistent Molecular Orbital Methods. XII. Further Extensions of Gaussian-Type Basis Sets for Use in Molecular Orbital Studies of Organic Molecules. *J. Chem. Phys.* **1972**, *56*, 2257−2261.
(46) Hellweg, A.; Hattig, C.; Hofener, S.; Klopper, W. Optimized Accurate Auxiliary Basis Sets for RI-MP2 and RI-CC2 Calculations for the Atoms Rb to Rn. *Theor. Chem. Acc.* **2007**, *117*, 587−597.
(47) Lu, T.; Chen, F. Multiwfn: A Multifunctional Wavefunction Analyser. *J. Comput. Chem.* **2012**, *33*, 580−592.
(48) Diamond−Crystal and Molecular Structure Visualization. http://www.crystalimpact.com/diamond (Accessed on 18 August 2022).
(49) Tanner, P. A.; Yeung, Y. Y.; Ning, L. What Factors Affect the $^5D_0$ Energy of Eu^{3+}? An Investigation of Nephelauxetic Effects. *J. Phys. Chem. A* **2013**, *117*, 2771−2781.
(50) Kasprzycka, E.; Carneiro Neto, A. N.; Trush, V. A.; Jerzykiewicz, L.; Amirkhanov, V. M.; Malta, O. L.; Legendziewicz, J.; Gawryszewska, P. How Minor Structural Changes Generate Major Consequences in Photophysical Properties of RE Coordination Compounds; Resonance Effect, LMCT State. *J. Rare Earths* **2020**, *38*, 552−563.
(51) Maple. *Maplesoft*; A Division of Waterloo Maple Inc.: Waterloo, Ontario, 2021.
(52) Henderson, B.; Imbusch, G. F. *Optical Spectroscopy of Inorganic Solids*; Oxford University Press: Oxford, U.K., 1989.
(53) Hilborn, R. C. Einstein Coefficients, Cross Sections, *f* Values, Dipole Moments and All That. *Am. J. Phys.* **1982**, *50*, 982−986.
(54) Dexter, D. L. A Theory of Sensitized Luminescence in Solids. *J. Chem. Phys.* **1953**, *21*, 836−850.
(55) Dodson, C. M.; Zia, R. *Magnetic Dipole and Electric Quadrupole Transitions in the Trivalent Lanthanide Series: Calculated Emission Rates and Oscillator Strengths*; Oxford University Press: Oxford, U.K., 1989.
(56) Bernath, P. F. MoLLIST: Molecular Line Lists, Intensities and Spectra. *J. Quant. Spectrosc. Radiat. Transfer* **2020**, *240*, No. 106687.
(57) Reid, M. F. Transition Intensities, Chapter 2, In *Crystal Field Handbook*; Cambridge University Press: Cambridge, 2000; Vol. *190*.
(58) Tanner, P. A. Spectra, Energy Levels and Energy Transfer in High Symmetry Lanthanide Compounds. *Top. Curr. Chem.* **2004**, *241*, 167−278.
(59) Rajamouli, B.; Devi, R.; Mohanty, A.; Krishnan, V.; Vaidyanathan, S. Effects of Electron-Withdrawing Groups in Imidazole-Phenanthroline Ligands and Their Influence on the Photophysical Properties of Eu^{III} Complexes for White Light-Emitting Diodes. *New J. Chem.* **2017**, *41*, 9826−9839.
(60) Brinen, J. S.; Halverson, F.; Leto, J. R. Photoluminescence of Lanthanide Complexes. IV. Phosphorescence of Lanthanum Compounds. *J. Chem. Phys.* **1965**, *42*, 4213−4219.
(61) Tanner, P. A.; Zhou, L.; Duan, C.-K.; Wong, K.-L. Misconceptions in Electronic Energy Transfer: Bridging the Gap between Chemistry and Physics. *Chem. Soc. Rev.* **2018**, *47*, 5234−5265.
(62) Chua, M.; Tanner, P. A.; Reid, M. F. Energy Transfer by Electric Dipole-Magnetic Dipole Interaction in Cubic Crystals. *Solid State Commun.* **1994**, *90*, 581−583.

https://doi.org/10.1021/acs.jpca.2c03965
J. Phys. Chem. A 2022, 126, 7418−7431